

## Article

# Wave-Current Loads on a Super-Large-Diameter Pile in Deep Water: An Experimental Study

Chenkai Hong <sup>1,2,\*</sup> , Zhongda Lyu <sup>2,\*</sup>, Fei Wang <sup>2</sup>, Zhuo Zhao <sup>2</sup> and Lei Wang <sup>1,2</sup><sup>1</sup> Faculty of Mechanical Engineering & Mechanics, Ningbo University, Ningbo 315211, China<sup>2</sup> Zhejiang Engineering Technology Research Center for Civil Engineering Industrialized Construction, Ningbo University of Technology, Ningbo 315211, China

\* Correspondence: hong\_chenkai@163.com (C.H.); lzd01@189.cn (Z.L.)

**Featured Application:** With the continuous development of marine engineering, super-large-diameter piles have been designed and constructed in deep water with complex and severe waves and currents. It is an important challenge in engineering design to determine wave and current loads of the super-large-diameter pile reasonably and accurately. However, the hydrodynamic coefficient given in the current design specifications are determined based on the model tests of small-diameter piles, which will no longer be applicable to the calculation of wave and current loads of super-large-diameter pile. In this article, taking one of the 6.3-m super-large-diameter piles of the main pier foundation of the Xihoumen Rail-cum-Road Bridge as the research object, we focused on the wave and current load characteristics and development laws of the super-large-diameter pile, and proposed the hydrodynamic coefficients of the super-large-diameter pile suitable for deep water, strong wave and current conditions. It can provide important reference for the engineering design of super-large-diameter pile for the foundation projects of cross-sea bridges, offshore platforms and offshore wind turbines in the future.

**Abstract:** Recently, the diameters and construction water depths of the pile foundations of planned and newly built sea-crossing bridges have been increasing greatly. Hydrodynamic loads are the key control factors in the design of super-large-diameter piles. However, most of the previous studies focused on the inline force on the pile with a small diameter, and there were few cases to consider the impact of the transverse force on the hydrodynamic load of the pile under wave-current actions. In this study, to understand the hydrodynamic loads on such deep-water super-large-diameter piles, the prototype was one of the 6.3-m piles used in the Xihoumen Rail-cum-Road Bridge, and 1:60-scale model tests were carried out in an experimental tank, with the actions of regular waves and waves combined with currents used as loads. The influence of the current velocity and static wave height on the inline and transverse forces on the pile was measured and analyzed. The experimental results indicate that with increasing current velocity, the fluctuation characteristics of the wave-current-induced inline and transverse forces change significantly, and their peak values increase obviously compared to those induced by only waves. In particular, the peak transverse force increases tens of times and can become equivalent to the inline force. The modified Morison formula and Kutta–Joukowski formula are used to derive the correlations between the drag coefficient  $C_D$ , inertia coefficient  $C_M$ , lift coefficient  $C_L$ , and redefined Keulegan–Carpenter number  $KC^*$ . Under wave-current action, the transverse force contributes quite significantly to the hydrodynamic load on a super-large-diameter pile, making it easier to trigger extreme structural loads. The results presented herein are an important reference for the engineering designs of such super-large-diameter piles.

**Keywords:** super-large-diameter pile; wave flume experiment; wave-current force; current velocity; wave height



**Citation:** Hong, C.; Lyu, Z.; Wang, F.; Zhao, Z.; Wang, L. Wave-Current Loads on a Super-Large-Diameter Pile in Deep Water: An Experimental Study. *Appl. Sci.* **2023**, *13*, 8859. <https://doi.org/10.3390/app13158859>

Academic Editor: Atsushi Mase

Received: 4 June 2023

Revised: 18 July 2023

Accepted: 29 July 2023

Published: 31 July 2023



**Copyright:** © 2023 by the authors. Licensee MDPI, Basel, Switzerland. This article is an open access article distributed under the terms and conditions of the Creative Commons Attribution (CC BY) license (<https://creativecommons.org/licenses/by/4.0/>).

## 1. Introduction

A deep understanding of the hydrodynamic loads on vertical piles induced by waves and currents is very important for designing marine structures such as sea-crossing bridges, offshore platforms, and wind farms [1–5]. As marine engineering develops gradually into deeper water and its scale expands continuously, pile foundations must withstand the huge forces associated with strong wave and current actions, which are the key control factors in the design and construction of such engineering structures. Therefore, a crucial issue for marine engineering design is accurate consideration of the wave-current loads on piles.

In practical engineering design, the influence of piles on wave propagation is usually ignored, with consideration given mainly to the viscous and added-mass effects of waves on structures. The classic Morison formula [6] is used to estimate the wave forces on piles, but the factors that influence the drag force coefficient  $C_D$  and inertia force coefficient  $C_M$  in the formula are very complicated and difficult to derive directly via theory, so instead these hydrodynamic coefficients are determined mainly via model experiments [7–11]. Sarpkaya and Storm [7] used oscillating flow in a U-shaped water tunnel to experiment on the wave force acting on a cylinder; they considered how  $C_D$  and  $C_M$  varied with the Reynolds number ( $Re$ ) and Keulegan–Carpenter number ( $KC = u_m T/D$ ), finding that the hydrodynamic coefficients of the cylinder differed under wave-only and wave-current conditions. Subsequently, Yu and Miao [8], Ren [9], and Li et al. [11,12] conducted hydrodynamic tests on piles under wave-only and wave-current actions; they calculated the hydrodynamic coefficients using the time-domain least-squares method and identified where in parameter space the drag and inertia forces were greatest. Wan et al. [13] used numerical methods to consider the conditions of fluid viscosity and low Reynolds number, and they obtained the stable hydrodynamic coefficients of a pile model under the combined actions of linear waves and currents.

Wave-current interactions can cause the forces acting on piles to change significantly [14]. Via flume model experiments, Ghadirian et al. [15] discussed how wave-current interactions affect the loads on piles, finding that the force coefficients under wave-current conditions are always lower than those under wave-only conditions. Via large-eddy simulations, Kang and Zhu [16] discussed the critical  $Re$  for a square pile under wave-current actions for  $KC = 0.6$  and  $Re = 1 \times 10^3$  to  $6 \times 10^5$ , where the drag coefficient and turbulence characteristics become more obvious when the critical  $Re$  is exceeded. Sundar et al. [17] reported how the drag and inertia coefficients varied with  $KC$  for an inclined pile, and Qu et al. [18] analyzed the wave force components in the frequency domain for a pile with different inclination angles. Via model experiments and numerical simulations, Corvaro et al. [19,20] analyzed the pressure distribution and total wave force on a pile under wave actions, as well as the generation and evolution of vortices around the pile; the results indicated that using the Morison formula with the finite-amplitude linear wave hypothesis to estimate the wave force on a pile under nonlinear wave action may result in significant errors, and also that the values of the drag and inertia coefficients are very uncertain at high Reynolds number ( $Re = 10^6$ – $10^7$ ). Furthermore, Miles et al. [21] conducted a quantitative model test on the turbulence distribution around a cylinder under a combination of waves and currents.

However, most of the above research was for piles with small diameters under either wave-only conditions or a combination of waves and low-speed currents, with more attention given to the inline force. In addition, there were few cases to reveal how the transverse force develops under wave-current action. Currently, the pile diameters of actual sea-crossing bridge foundations are changing greatly, increasing from less than 2 m to more than 6 m, and meanwhile, the construction conditions are shifting from inshore river estuaries with shallow water and relatively moderate waves and currents to fjord waterways with deeper water, high waves, and rapid currents, thereby making the marine-environment challenges for construction more complex and severe. Therefore, there is an urgent need for further research into wave-current loads and their development patterns for

super-large-diameter piles in the deep-water foundations of modern sea-crossing bridges under the combined action of strong waves and currents.

The Xihoumen Strait is a well-known area of rapids in China, with a 100-year return period and a current rate of 3.3 m/s. Currently under construction, the Xihoumen Rail-cum-Road Bridge uses 18 piles with a super-large diameter of 6.3 m for the foundation of its main tower, built on the seabed composed of bedrock with a water depth of 60 m, as shown in Figure 1. Globally, this pile diameter and construction water depth are the largest to date in the construction of pile foundations for sea bridges; they are more than twice those for the foundations of the existing Hangzhou Bay Bridge and East Sea Bridge in China, and they exceed the 4.5-m pile diameter and 45-m construction water depth of the main pier of the Pingtan Straits Rail-cum-Road Bridge.

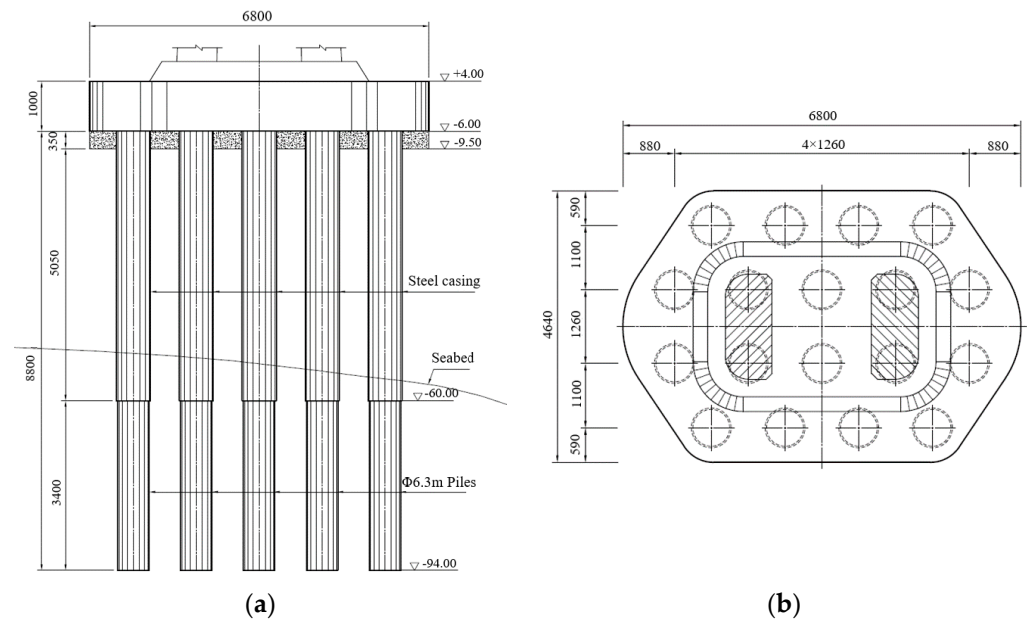


**Figure 1.** Schematics of the foundation of the Xihoumen Rail-cum-Road Bridge: (a) sectional view; (b) plan view (unit: cm).

The aims of this study are to (i) give insights into the characteristics of wave–current loads on super-large-diameter piles in deep water and under strong waves and currents and (ii) explore a practical method for calculating such loads. Taking one of the 6.3-m super-large-diameter piles of the Xihoumen Rail-cum-Road Bridge as the research object, this paper begins by considering the variation laws and influencing factors for the force on the pile under the actions of regular waves either alone or combined with a uniform current in the same direction as determined via flume model experiments. Then, based on the modified Morison formula and linear wave theory, the hydrodynamic coefficients  $C_D$ , and  $C_M$  of the super-large-diameter pile under wave-current actions are derived and analyzed using the least-squares method. In addition, the lift coefficient  $C_L$  of the super-large-diameter pile under wave–current actions is derived and analyzed based on the Kutta–Joukowski formula. Finally, how the transverse force influences the peak value and direction of the resultant force is analyzed.

## 2. Experimental Design and Setup

### 2.1. Model of a Super-Large-Diameter Pile

The experiments were conducted in the Laboratory of Offshore Engineering at Zhejiang University of Technology in China. The wave flume was 75 m long, 1.8 m wide, and 2 m deep, and the maximum allowable operating depth of water was 1.5 m. As shown in Figure 2, a hydraulic-piston wave generator at one end of the flume generated one-way waves, and an absorber beach made of porous polymer material at the other end absorbed most of the

incident waves and reduced wave reflection. Furthermore, with an inlet and an outlet at the bottom of the two ends of the flume, uniform currents could be generated by a circulation pump system.

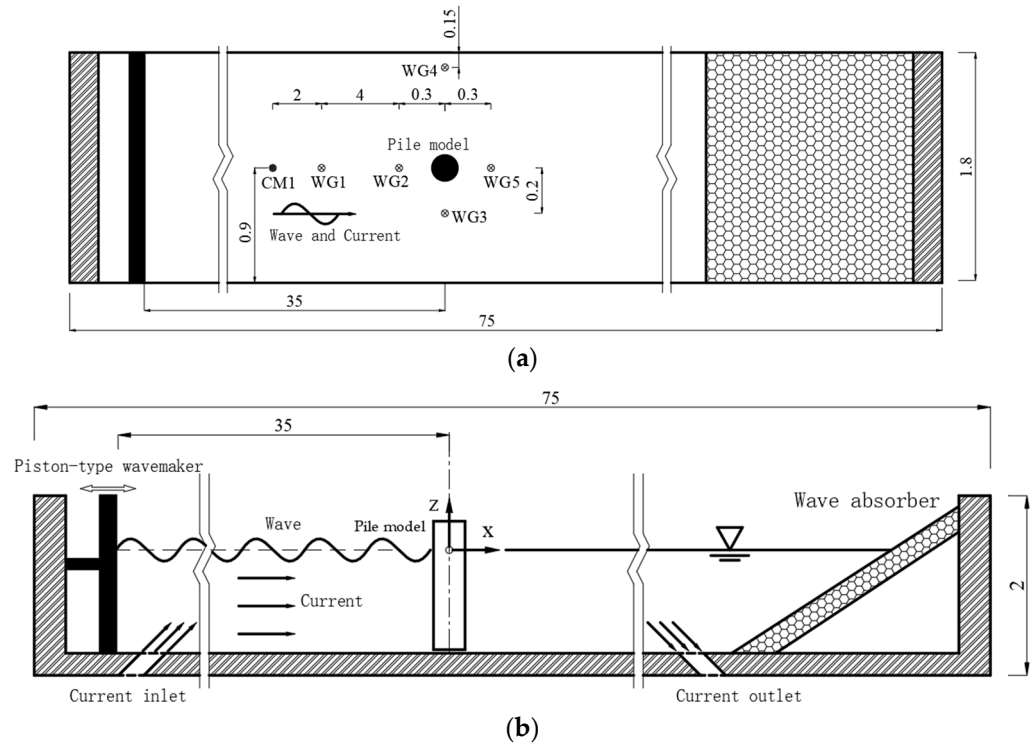


Figure 2. Schematics of the wave flume: (a) plan view; (b) side view (unit: m).

Taking one of the 6.3-m super-large-diameter piles of the main pier foundation of the Xihoumen Rail-cum-Road Bridge as a reference and ignoring the part of the pile that is embedded into the rock, the experimental prototype was designed as a super-large-diameter pile with a diameter of 6.3 m and a length of 72 m in 60 m deep water. To compare the variation laws for the hydrodynamic loads on piles with different diameters, another two piles were designed with diameters of 4.5 m and 2.7 m. Considering (i) the size of the wave flume, (ii) the wave and current conditions, and (iii) the geometric and Froude similarity criteria, the experimental model was designed at a model scale of 1:60 (model: prototype); as shown in Figure 3, the diameters of the pile models were 10.5 cm, 7.5 cm, and 4.5 cm, respectively, and their length was 120 cm.

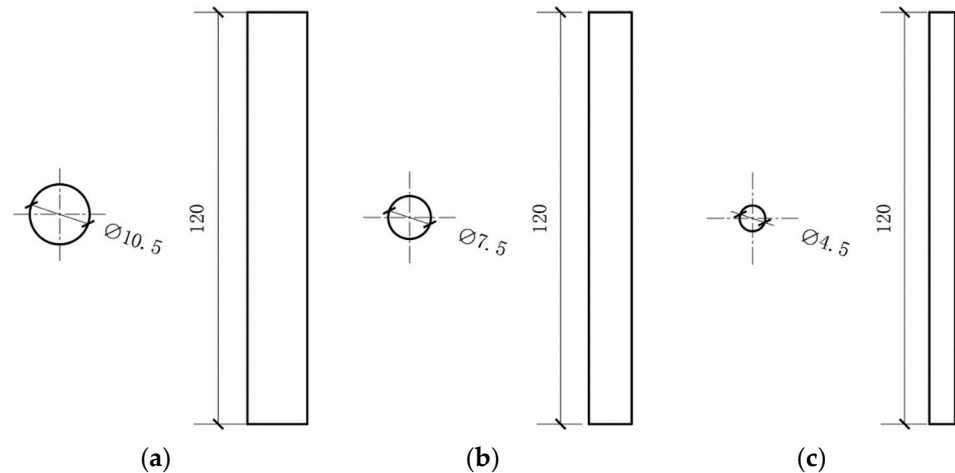
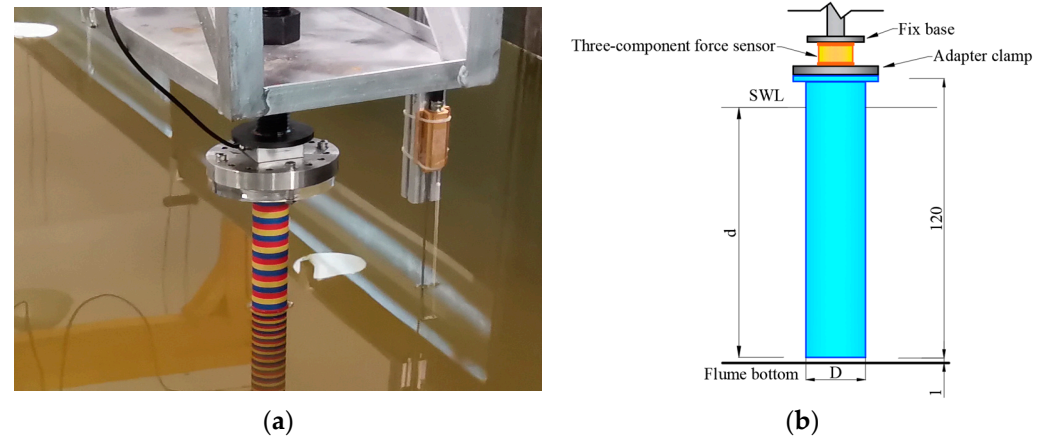


Figure 3. Single-pile models: (a)  $D = 10.5$  cm; (b)  $D = 7.5$  cm; (c)  $D = 4.5$  cm.

Each test specimen was made of acrylic, which is internally hollow and fully closed. As shown in Figure 2, the studied specimen was installed rigidly about 35 m from the wave maker, and as shown in Figure 4, the upper end of the specimen was connected to a three-component force sensor installed on a steel frame. The bottom of the pile was kept 1 cm from the floor of the wave flume to ensure that the measured forces on the pile were unaffected by the floor.



**Figure 4.** Installation of pile model: (a) photograph of model in wave flume; (b) measurement arrangement (unit: cm).

## 2.2. Testing Conditions

The water depth and wave-current conditions in the flume were designed to realistically simulate the conditions found in the Xihoumen Strait of China. Based on the model scale, the experiments simulated the conditions of regular waves and currents at the corresponding constant water depth of  $d = 1.0$  m.

Over a 100-year return period in the Xihoumen Strait, the wave heights at cumulative frequencies of 1%, 5%, and 13% and the average wave height were 7.80 m, 6.37 m, 5.32 m, and 3.36 m, respectively; the average wave period was 10.4 s and the current rate was 3.3 m/s. Based on these wave and current conditions, 20 different test cases of wave and current combinations acting in the same direction were designed, and the wave and current parameters of the model and prototype are given in Table 1.

**Table 1.** Wave and current parameters.

Model			Prototype		
$H_0$ [cm]	$T$ [s]	$U$ [m/s]	$H_p$ [m]	$T_p$ [s]	$U_p$ [m/s]
5.6	1.35	0, 0.1, 0.2, 0.3, 0.4	3.36	10.4	0, 0.8, 1.6, 2.5, 3.3
8.9	1.35	0, 0.1, 0.2, 0.3, 0.4	5.32	10.4	0, 0.8, 1.6, 2.5, 3.3
10.6	1.35	0, 0.1, 0.2, 0.3, 0.4	6.37	10.4	0, 0.8, 1.6, 2.5, 3.3
13.0	1.35	0, 0.1, 0.2, 0.3, 0.4	7.80	10.4	0, 0.8, 1.6, 2.5, 3.3

Notes:  $H_0$ —model wave height [cm] under wave action without current;  $T$ —model wave period [s] under wave action without current;  $U$ —model current velocity [m/s] under current-only action.

In these experiments, the wave and current conditions were generated using the same methods as those used by Chen et al. [22] and Kang et al. [23]. In the wave-only case, regular waves were generated by the reciprocal motion of the wave maker; in the current-only case, a uniform current was generated by adjusting the flow rate of the circulation pump system until the velocity of the current was stable; in the wave-current case, the current was generated first, then the wave generator was run using the same control parameters as those in the wave-only case. The wave-current forces on the pile were measured when the waves and the current had been combined stably; each case was repeated three times to reduce random experimental errors, and the test results presented herein are the average values of those three tests.

### 2.3. Instrumentation and Data Sampling

A three-component force sensor (FC3D80, produced by Forcechina Measurement Technology Co., Ltd., Shanghai, China) installed as shown in Figure 4b was used to measure the wave/wave-current forces on the pile model. The calibrated sensor had the following performance-related characteristics:  $F_x$  and  $F_y$  were in the range of  $\pm 150$  N at a resolution of 0.015 N, and  $F_z$  was in the range of  $\pm 300$  N at a resolution of 0.03 N, where  $F_x$  is the inline force in the direction of wave propagation,  $F_y$  is the transverse force perpendicular to the direction of wave propagation, and  $F_z$  is the vertical force.

To investigate the wave propagation, five capacitance-type wave gauges (WG1–WG5) with a precision of 0.1 mm and a sampling rate of 200 Hz were arranged at different positions in the water flume, as shown in Figure 2a: WG1 was 4.3 m upstream of the pile model to measure the incident waves; WG2, WG3, and WG5 measured wave fluctuations around the model; WG4 measured waves 0.15 m from the side wall of the flume and at the horizontal position of the center of the model.

As shown in Figure 2a, an acoustic Doppler velocimeter (ADV) [labeled CM1 in Figure 2a] with an accuracy of 0.5% and a sampling frequency of 100 Hz was used to measure the velocity of the current. The ADV, the three-component force sensor, and all the wave gauges were calibrated prior to the experiments.

## 3. Effect of Current on Wave Height

### 3.1. Analytical Solution for Current-Affected Wave Height

Studying how a coexisting current affects the wave characteristics (e.g., wave height and wavelength) is beneficial for gaining a deeper understanding of the mechanism of wave-current action on structures, and research into how the wave characteristics change under the action of a current has yielded several achievements [24–26]. Assuming uniform flow and based on linear wave theory and the conservation of wave action, Li and Herbich [24] provided a relatively accurate analytical solution for the current-affected wave height  $H$ , i.e.,

$$\frac{H}{H_0} = \left(1 - \frac{U}{C}\right)^{0.5} \left(\frac{L_0}{L}\right)^{0.5} \left(\frac{A_0}{A}\right)^{0.5} \left(1 + \frac{U}{C} \frac{2-A}{A}\right)^{0.5} \quad (1)$$

$$\frac{L}{L_0} = \frac{c}{c_0} = \left(1 - \frac{U}{c}\right)^{-2} \frac{\tanh kd}{\tanh k_0 d} \quad (2)$$

$$A_0 = 1 + \frac{2k_0 d}{\sinh 2k_0 d} \quad (3)$$

$$A = 1 + \frac{2kd}{\sinh 2kd} \quad (4)$$

where  $L$ ,  $k$ , and  $A$  are the wavelength, wave number, and wave energy transmissivity, respectively. The subscript 0 denotes parameters under wave action with no current,  $U$  is the current velocity,  $C$  is the wave celerity in the current, and  $d$  is the water depth. Equations (1)–(4) are all related to the wave number  $k$  under wave-current action, and the modified dispersion relation is as follows:

$$\left(\frac{2\pi}{T} - kU\right)^2 = gk \tanh kd \quad (5)$$

### 3.2. Data Analysis of Current-Affected Wave Height

Wave heights were measured with different current velocities, and Figure 5 shows representative time series of wave elevation for  $H_0 = 8.9$  cm and 13.0 cm,  $T = 1.35$  s, and  $U = 0$  m/s, 0.1 m/s, and 0.4 m/s. Compared to that under wave-only action, the wave amplitude decreases obviously under wave-current action, while the wave period remains nearly constant.

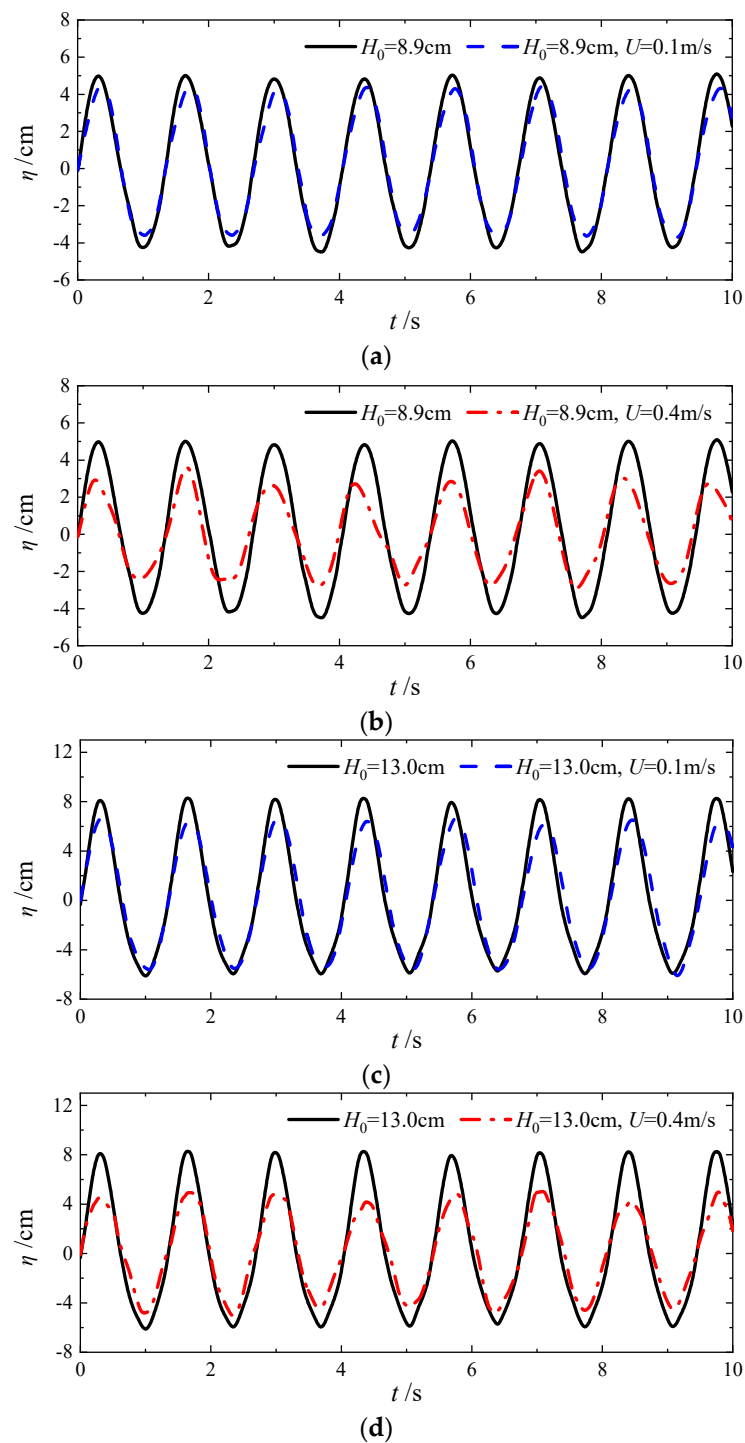


**Figure 5.** Time series of wave elevation: (a)  $H_0 = 8.9$  cm,  $U = 0$  or  $0.1$  m/s; (b)  $H_0 = 8.9$  cm,  $U = 0$  or  $0.4$  m/s; (c)  $H_0 = 13.0$  cm,  $U = 0$  or  $0.1$  m/s; (d)  $H_0 = 13.0$  cm,  $U = 0$  or  $0.4$  m/s.

Figure 6 shows the current-affected wave height decreasing gradually as the current velocity increases. Compared with the wave height under wave-only conditions ( $H_0 = 8.9$  cm and  $13.0$  cm), the current-affected wave height  $H$  decreases by about 8% and 9% for  $U = 0.1$  m/s and by about 31% and 30% for  $U = 0.4$  m/s. In addition, Equations (1)–(5) are used to compare the measured wave height variation with the theoretical calculation results; the error between the two is about 5% at most, which occurs for  $H = 8.9$  cm,  $T = 1.35$  s, and  $U = 0.4$  m/s. This indicates that Equation (1) offers an accurate estimation of the design

wave height in actual engineering environments under the combination of deep water, strong waves, and rapid current.

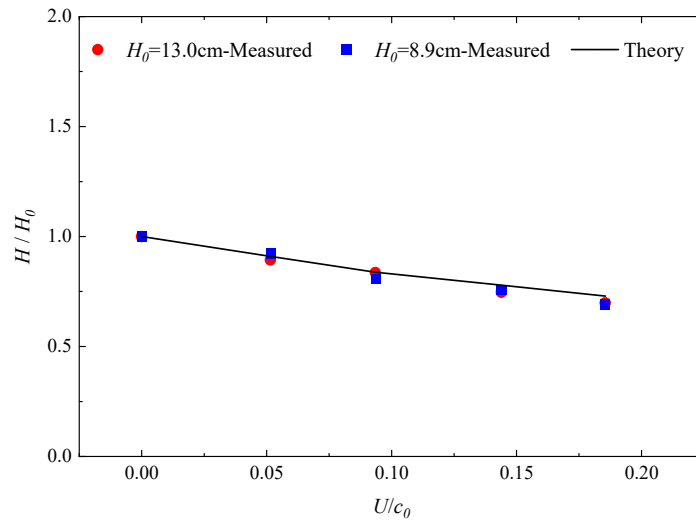


Figure 6. Wave height change versus relative current velocity  $U/c_0$  for  $U = 0\text{--}0.4$  m/s.

#### 4. Wave–Current Force on Pile

##### 4.1. Calculation Theory of Wave-Current Force and Hydrodynamic Coefficient of Pile

According to the analysis in Section 3, it is assumed that (i) the current-affected wave retains linear wave characteristics and (ii) only the wave height  $H$  changes. In that case, the wave surface elevation  $\eta$  can be expressed as

$$\eta = \frac{H}{2} \sin(kx - \omega t) \tag{6}$$

where  $H$  and  $k$  are the current-affected wave height and wave number, respectively, and  $\omega = 2\pi/T$  is the angular frequency. The horizontal and vertical velocities of a water particle affected by a uniform current are:

$$u_x = U + \frac{H}{2}(\omega - kU) \frac{\cosh k(z + d)}{\sinh kd} \cos(kx - \omega t) \tag{7}$$

$$u_z = \frac{H}{2}(\omega - kU) \frac{\sinh k(z + d)}{\sinh kd} \sin(kx - \omega t) \tag{8}$$

To consider the impact of hydrodynamic loads, the modified Morison formula and Kutta–Joukowski formula proposed by Iwagaki and Asano [27] were used to evaluate the inline and transverse forces on the pile, i.e.,

$$F_x = \int \frac{1}{2} C_D \rho A (u_w + U) |u_w + U| dz + \int C_M \rho V \dot{u}_w dz \tag{9}$$

$$F_y = \int \frac{1}{2} C_L \rho D (u_w + U)^2 dz \tag{10}$$

where  $F_x$  and  $F_y$  are the inline and transverse forces acting on the pile, respectively.  $C_D$ ,  $C_M$ , and  $C_L$  are the drag, inertia, and lift coefficients, respectively.  $\rho$  is the fluid density,  $A$  is the projection area of the pile perpendicular to the wave propagation,  $V$  is the volume of the pile immersed in the fluid,  $D$  is the pile diameter,  $u_w$  is the wave-induced horizontal particle velocity, and  $\dot{u}_w$  is the horizontal particle acceleration.

The resultant force  $F_H$  on the pile is the vector sum of  $F_x$  and  $F_y$ , i.e.,

$$F_H = (F_x^2 + F_y^2)^{0.5} \quad (11)$$

The theoretical inline, transverse, and resultant forces on the pile can be calculated using Equations (7)–(11). Then the hydrodynamic coefficients  $C_D$  and  $C_M$  can be calculated by the least-squares method, with  $C_L$  determined using Equation (10).

Previous research experience suggests that the hydrodynamic coefficients ( $C_D$ ,  $C_M$ , and  $C_L$ ) are closely related to  $KC$  [7–9,11,16]. Therefore, herein, the redefined  $KC^*$  for wave-current conditions is used to characterize the hydrodynamic coefficients, i.e.,

$$\begin{cases} KC^* = \frac{u_m T}{D} [\sin \varphi + (\pi - \varphi) \cos \varphi], & |U| < u_m \\ KC^* = \frac{\pi |U| T}{D}, & |U| \geq u_m \end{cases} \quad (12)$$

where  $\varphi = \arccos \frac{|U|}{u_m}$ , and the maximum horizontal velocity of particles induced by waves is  $u_m = \frac{\pi H}{T} \coth kd$ .

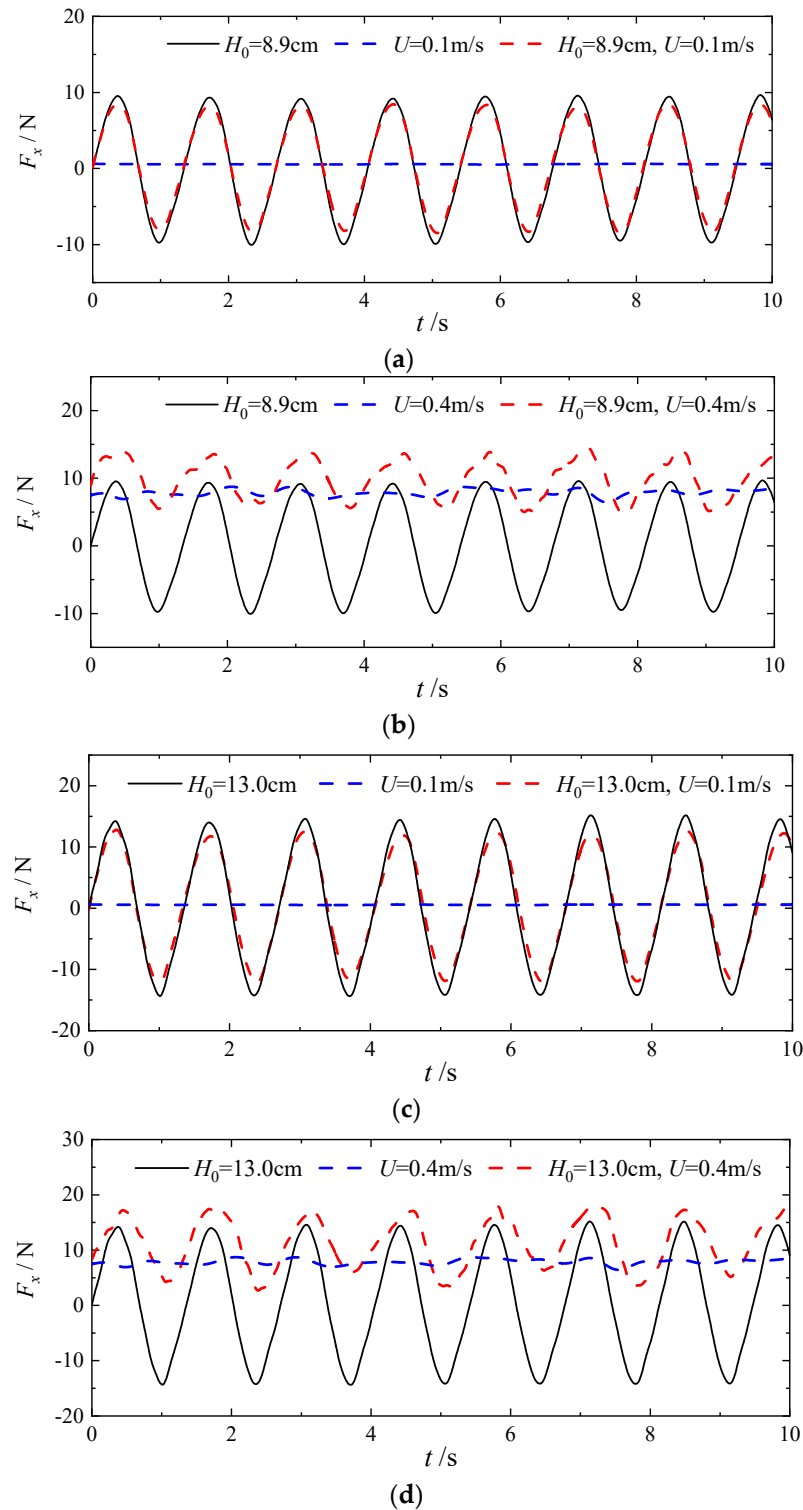
#### 4.2. Typical Wave-Current Force Time Series

To investigate the variation patterns and influencing factors of the hydrodynamic loads on a super-large-diameter pile, the inline and transverse forces for the 20 different wave-current combinations listed in Table 1 were studied. Figures 7 and 8 show representative time series of the inline and transverse forces on the pile with  $D = 10.5$  cm in the wave-only, current-only, and wave-current cases. As can be seen, the inline and transverse forces induced by wave-current action differ from those induced by wave-only action, and this phenomenon is more pronounced as the current becomes faster.

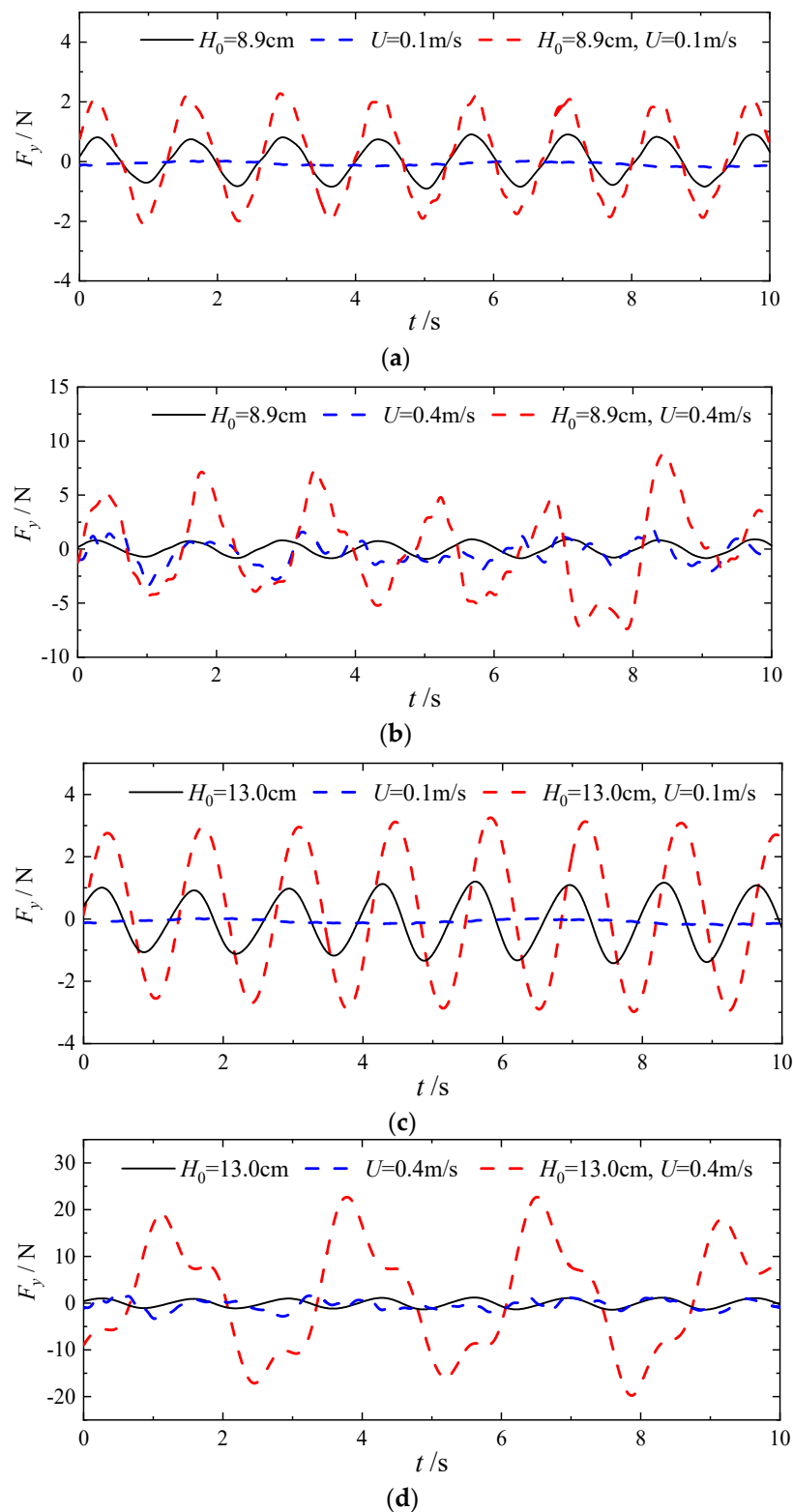
Figure 7a,c show that compared with the corresponding wave-only cases, when waves with  $H_0 = 8.9$  cm and 13.0 cm and  $T = 1.35$  s are combined with a current of  $U = 0.1$  m/s, the mean values of the inline force time histories are still near zero, but the wave amplitudes decrease by ca. 14%. Figure 7b,d suggest that for the combined wave-current cases of  $H_0 = 8.9$  cm and 13.0 cm and  $U = 0.4$  m/s, the mean values of the inline force time histories are 9.6 N and 10.3 N, respectively, which are closer to that induced in the current-only case of  $U = 0.4$  m/s and significantly greater than zero. The amplitudes decrease by more than 50%, and the trough value exceeds zero. These results indicate that when the current is slow, it does not change the intensity and peak value of the inline force fluctuation significantly, but when the current is faster, it decreases the intensity of the inline force fluctuation significantly, while the peak value increases and enhances the nonlinearity of the fluctuations.

Figure 8 compares the measured time histories of the transverse force on the pile with  $D = 10.5$  cm for  $H_0 = 8.9$  cm and 13.0 cm,  $T = 1.35$  s, and  $U = 0$  m/s, 0.1 m/s, and 0.4 m/s. As can be seen, the wave-current-induced transverse force is significantly greater than that induced by waves alone or current alone. When the current velocity  $U$  is relatively small, the fluctuation amplitude of the transverse force induced by wave-current action (the cases of  $H_0 = 8.9$  cm,  $U = 0.1$  m/s and  $H_0 = 13.0$  cm,  $U = 0.1$  m/s) increases significantly by ca. 150% and 180%, respectively, compared with that induced by wave-only action (the cases of  $H_0 = 8.9$  cm and 13.0 cm); meanwhile, the fluctuation periods do not change remarkably and the fluctuation patterns are almost symmetric, as shown in Figure 8a,c (where  $U = 0.1$  m/s). As the current becomes faster, the transverse force time series becomes more complex. The fluctuation amplitude of the transverse force induced by wave-current action (the cases of  $H_0 = 8.9$  cm,  $U = 0.4$  m/s and  $H_0 = 13.0$  cm,  $U = 0.4$  m/s) increases sharply to nearly 6.7 and 18.5 times that induced by wave-only action (the cases of  $H_0 = 8.9$  cm and 13.0 cm), respectively; see Figure 8b,d. In addition, the fluctuation period of the transverse force induced by wave-current action is about 1.5 and 2.0 times that induced by wave-only action, respectively. Moreover, the peaks and troughs of the transverse force fluctuations are not

symmetric, and the wave patterns within adjacent periods are also inconsistent. That is because, according to Kelvin circulation theory, the flow boundary layer separates with increasing  $Re$  associated with high current velocity, and asymmetric vortices appear around the pile; this leads to the flow field having significantly greater transverse asymmetry, resulting in the pressure on the pile surface being distributed much more asymmetrically.



**Figure 7.** Typical time histories of inline force on pile ( $D = 10.5$  cm) due to wave-only (black solid line), current-only (blue dotted line), and wave-current (red dotted line) conditions: (a)  $H_0 = 8.9$  cm,  $U = 0.1$  m/s; (b)  $H_0 = 8.9$  cm,  $U = 0.4$  m/s; (c)  $H_0 = 13.0$  cm,  $U = 0.1$  m/s; (d)  $H_0 = 13.0$  cm,  $U = 0.4$  m/s.



**Figure 8.** Typical time histories of transverse force on a pile ( $D = 10.5\text{ cm}$ ) due to wave-only (black solid line), current-only (blue dotted line), and wave-current (red dotted line) conditions: (a)  $H_0 = 8.9\text{ cm}$ ,  $U = 0.1\text{ m/s}$ ; (b)  $H_0 = 8.9\text{ cm}$ ,  $U = 0.4\text{ m/s}$ ; (c)  $H_0 = 13.0\text{ cm}$ ,  $U = 0.1\text{ m/s}$ ; (d)  $H_0 = 13.0\text{ cm}$ ,  $U = 0.4\text{ m/s}$ .

Overall, affected by the strong forward current, the wave-current-induced inline and transverse forces are significantly greater than those induced by only waves, and the transverse wave-current force increases to the same level as the inline wave-current force. Therefore, when designing the strength of this type of super-large-diameter pile, the

current effect and the significant transverse force should be taken into account, which are significantly different from the wave-induced horizontal force.

### 4.3. Wave-Current Force Analysis

#### 4.3.1. Effects of Current Velocity

To investigate how the current velocity affects the wave-current forces on the pile, Figures 9 and 10 compare the peak values of the inline and transverse wave-current forces on the three pile columns (i.e.,  $D = 4.5$  cm, 7.5 cm, and 10.5 cm) at a water depth of  $d = 1.0$  m and the wave-current parameters of  $H_0 = 8.9$  cm and 13.0 cm,  $T = 1.35$  s, and  $U = 0-0.4$  m/s ( $U/c_0 = 0-0.194$ ).

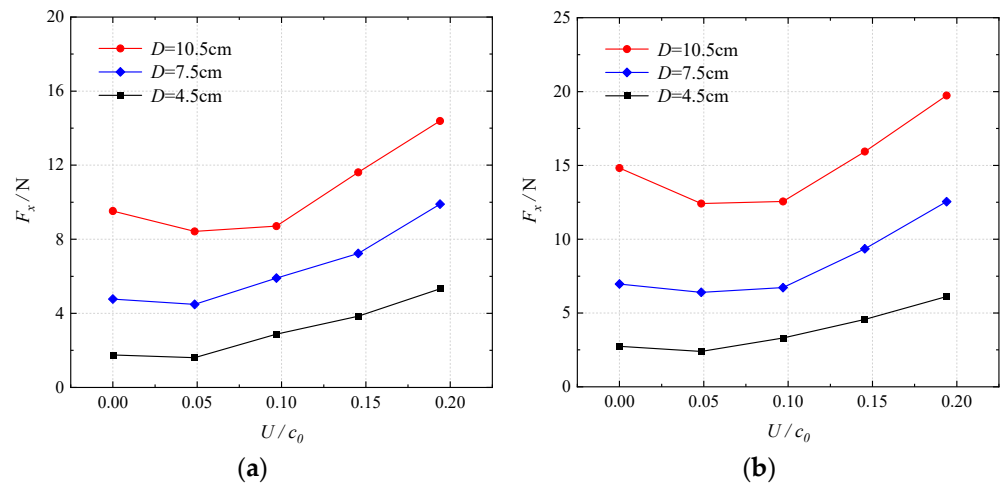


**Figure 9.** Inline wave-current forces on single-pile models versus relative velocity: (a)  $H_0 = 8.9$  cm,  $U/c_0 = 0-0.194$ ; (b)  $H_0 = 13.0$  cm,  $U/c_0 = 0-0.194$ .

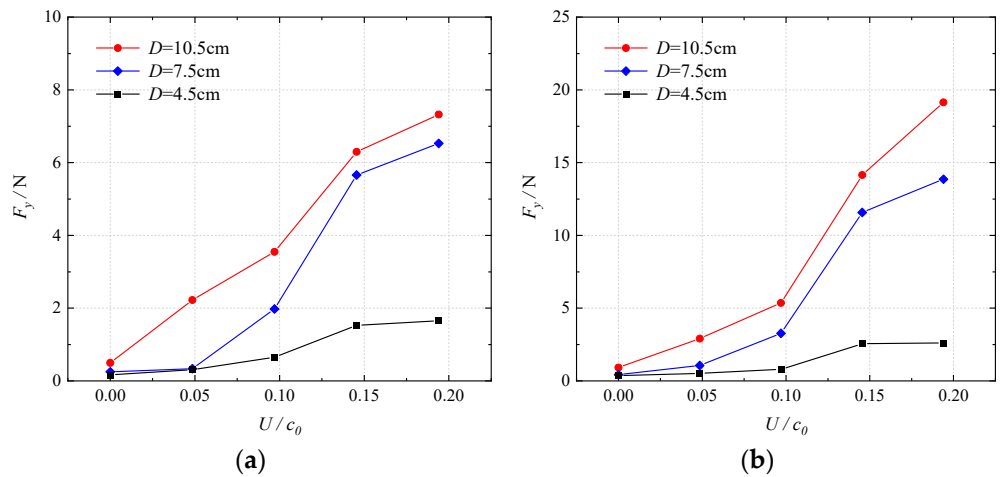


**Figure 10.** Transverse wave-current forces on single-pile models versus relative velocity: (a)  $H_0 = 8.9$  cm,  $U/c_0 = 0-0.194$ ; (b)  $H_0 = 13.0$  cm,  $U/c_0 = 0-0.194$ .

As shown in Figure 9, when the current is relatively slow ( $U = 0.1$  m/s), the current-affected wave height is reduced compared to that of pure waves, which means that the energy of the flow field is reduced. However, the increase in the velocity of water particles in the  $x$ -direction due to the current effect is not enough to offset the decrease in inline force caused by the decrease in wave height. Therefore, the peak inline force  $F_x$  on the pile under the combination of waves and a slow current is slightly less than that under wave-only conditions. As the current becomes faster ( $U = 0.3-0.4$  m/s), although the current-affected wave height decreases further, the faster water particles in the  $x$ -direction make a more significant contribution to the forward wave flow force in the whole water depth. The

peak value of the inline wave-current force  $F_x$  is significantly higher than that induced by pure waves ( $U = 0$  m/s), and the increase rate of the peak value accelerates obviously as the current velocity increases. For the pile with  $D = 10.5$  cm, the wave-current-induced inline forces for the cases of  $H_0 = 8.9$  cm,  $U = 0.4$  m/s and  $H_0 = 13.0$  cm,  $U = 0.4$  m/s, increase by ca. 51% and 31%, respectively, compared to the wave-only forces (for the cases of  $H_0 = 8.9$  cm and 13.0 cm).

The variation trends of inline wave-current force  $F_x$  versus current velocity for the three piles are different. In the current velocity range of  $U = 0.2$ – $0.4$  m/s, the larger the pile diameter, the more obvious the upward trend of the forward wave-current force, as shown in Figure 9a,b. In addition, because of the current effect, when the current velocity reaches  $U = 0.1$  m/s, the peak value of the inline wave-current force  $F_x$  increases rapidly for the pile with  $D = 4.5$  cm, while for the pile with  $D = 10.5$  cm, the growth rate of the peak value of  $F_x$  accelerates obviously when the flow velocity  $U$  exceeds 0.2 m/s, lagging behind that for the pile with  $D = 4.5$  cm.

Figure 10 shows that, similar to the inline wave-current force, the peak values of the transverse wave-current force  $F_y$  on the three piles increase as the current becomes faster, and the growth trend becomes more significant as the pile diameter increases. Compared with that under wave-only conditions or the combination of waves and a slow current,  $F_y$  increases greatly under the combination of waves and a fast current, and the increase can be by a factor of several tens. For  $H_0 = 13.0$  cm and  $U = 0.4$  m/s, the peak transverse forces on the piles with  $D = 4.5$  cm, 7.5 cm, and 10.5 cm are ca. seven, 31, and 20 times those under wave-only conditions, respectively. This indicates that the current velocity is an important factor affecting the increase of the transverse wave-current force.

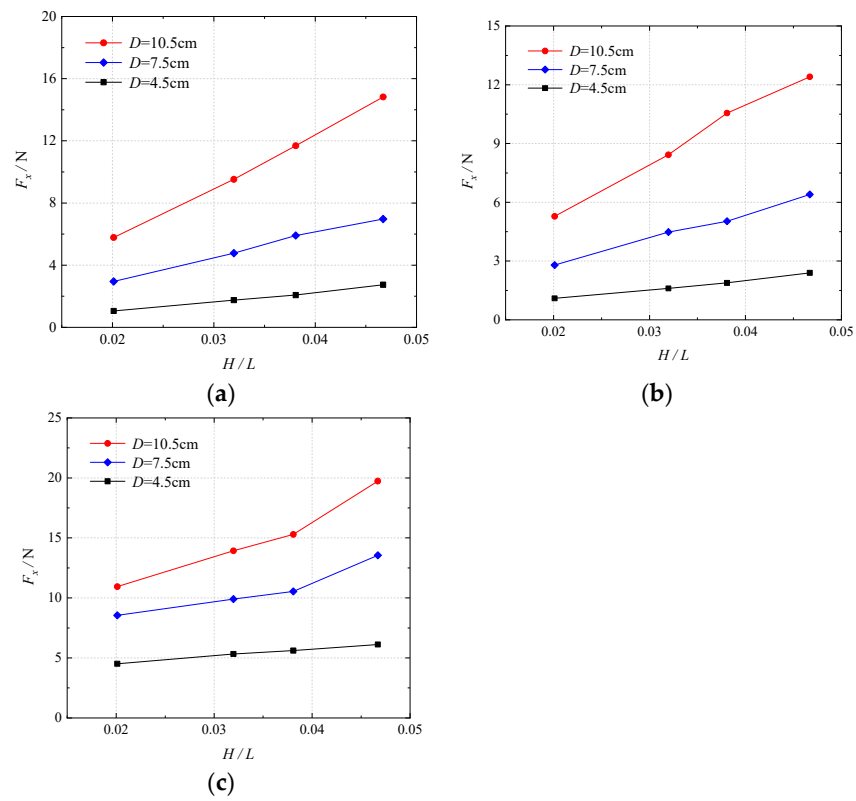
Moreover, comparing Figures 9b and 10b shows that the peak transverse force on the pile can reach the same value as the peak inline force under the combination of a strong wave and a strong current (i.e.,  $H_0 = 13.0$  cm and  $U = 0.4$  m/s). This is most obvious for the super-large-diameter pile with  $D = 10.5$  cm, for which the peak transverse force is about 98% of the peak positive force for  $H_0 = 13.0$  cm and  $U = 0.4$  m/s.

#### 4.3.2. Effects of Wave Height

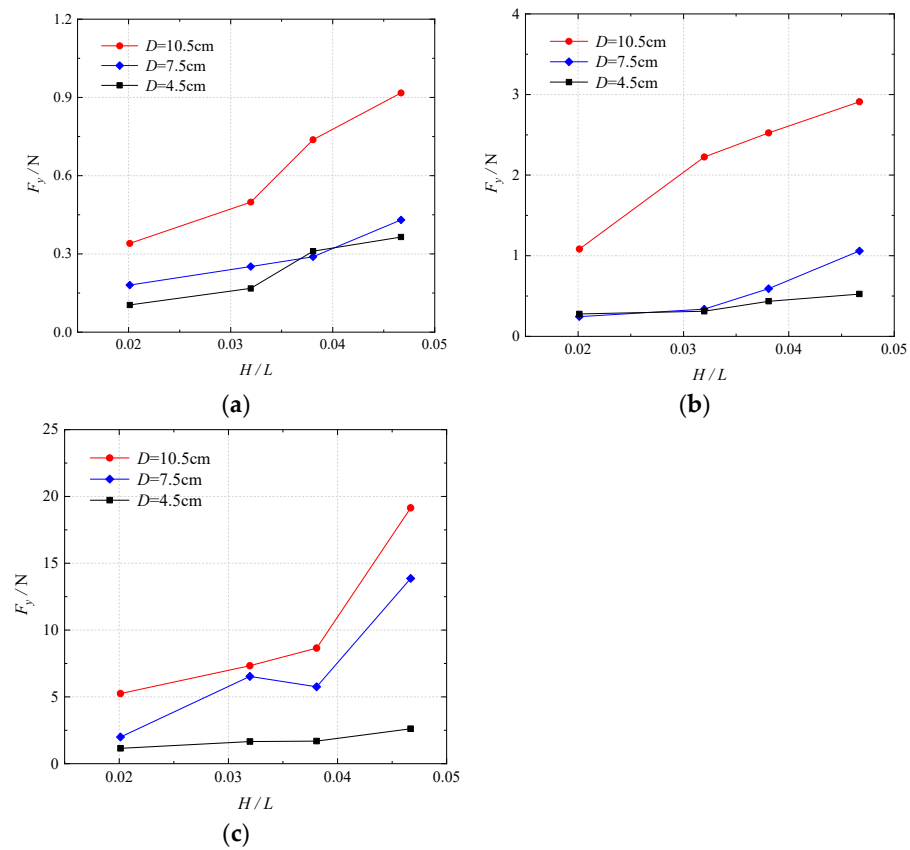
To investigate how the wave height affects the pile wave-current forces, Figures 11 and 12 compare the peak values of the inline and transverse wave-current forces on the three piles (i.e.,  $D = 4.5$  cm, 7.5 cm, and 10.5 cm) at water depth  $d = 1.0$  m and the wave-current parameters of  $U = 0$  m/s, 0.1 m/s, and 0.4 m/s and  $H_0 = 5.6$ – $13.0$  cm ( $H_0/L = 0.020$ – $0.047$ ).

Figure 11 shows that with increasing wave height, the peak inline forces on all three piles increase. For  $U = 0$  m/s and 0.1 m/s, the peak values of the inline force  $F_x$  on the three piles increase approximately linearly with increasing wave height. For  $U = 0.4$  m/s, the peak value of the inline force on the pile with  $D = 4.5$  cm still increases approximately linearly with increasing wave height, but for the larger-diameter piles with  $D = 7.5$  cm and 10.5 cm, the growth rate of the peak inline forces increases obviously when the wave height exceeds  $H_0 = 10.6$  cm. Meanwhile, for  $U = 0.4$  m/s and  $H_0 = 5.6$ – $13.0$  cm, the peak values of the inline wave forces on the piles with  $D = 4.5$  cm, 7.5 cm, and 10.5 cm increased by ca. 36%, 58%, and 80%, respectively. This indicates that with a nonlinear wave flow field comprising strong waves and current, it is easier to excite an extreme inline wave-current force on a pile with a super-large-diameter than on one with a smaller diameter.

Figure 12 shows that with increasing wave height, the peak transverse forces on all three piles increase. In particular, for  $U = 0.4$  m/s, the peak values of the inline force on the piles with  $D = 4.5$  cm, 7.5 cm, and 10.5 cm for  $H_0 = 13.0$  cm are about 2.2, 6.8, and 3.7 times those for  $H_0 = 5.6$  cm, respectively (Figure 12c). Under the combination of waves and a fast current, the increasing trend of the transverse force on the larger-diameter piles ( $D = 7.5$  cm and 10.5 cm) is more significant than that on the smaller-diameter pile ( $D = 4.5$  cm).



**Figure 11.** Inline wave–current forces on pile models versus wave steepness: (a)  $U = 0\text{ m/s}$ ,  $H_0/L = 0.020\text{--}0.047$ ; (b)  $U = 0.1\text{ m/s}$ ,  $H_0/L = 0.020\text{--}0.047$ ; (c)  $U = 0.4\text{ m/s}$ ,  $H_0/L = 0.020\text{--}0.047$ .



**Figure 12.** Transverse wave–current forces on pile models versus wave steepness: (a)  $U = 0\text{ m/s}$ ,  $H_0/L = 0.020\text{--}0.047$ ; (b)  $U = 0.1\text{ m/s}$ ,  $H_0/L = 0.020\text{--}0.047$ ; (c)  $U = 0.4\text{ m/s}$ ,  $H_0/L = 0.020\text{--}0.047$ .

In general, both current velocity and wave height are important factors affecting the inline and transverse forces on a pile. For a super-large-diameter pile in particular, the peak wave-current force growth trend is more significant as the current velocity and wave height increase. Meanwhile, the combination of strong waves and current is more likely to excite inline and transverse ultimate wave-current loads on such a structure. In addition, the large peak value of the transverse force will inevitably have a significant influence on the hydrodynamic load characteristics of the pile. Therefore, in the engineering design, sufficient attention should be paid to the transverse wave-current load on such a super-large-diameter pile in deep water under the combination of strong waves and current.

4.4. Analysis of Hydrodynamic Coefficients

To understand further the hydrodynamic load characteristics of a super-large-diameter pile in deep water, the modified Morison formula [Equation (9)] and Kutta–Joukowski formula [Equation (10)] were used to evaluate the drag, inertia, and lift coefficients of the three piles ( $D = 4.5$  cm,  $7.5$  cm, and  $10.5$  cm) under combined wave-current action.

4.4.1. Data Dispersion Analysis

Similar to the experimental results of Li et al. [11,12] and Iwagaki et al. [27], in this study the drag coefficient  $C_D$  (see Figure 13), inertia coefficient  $C_M$  (see Figure 14), and lift coefficient  $C_L$  (see Figure 15) are also somewhat dispersed.

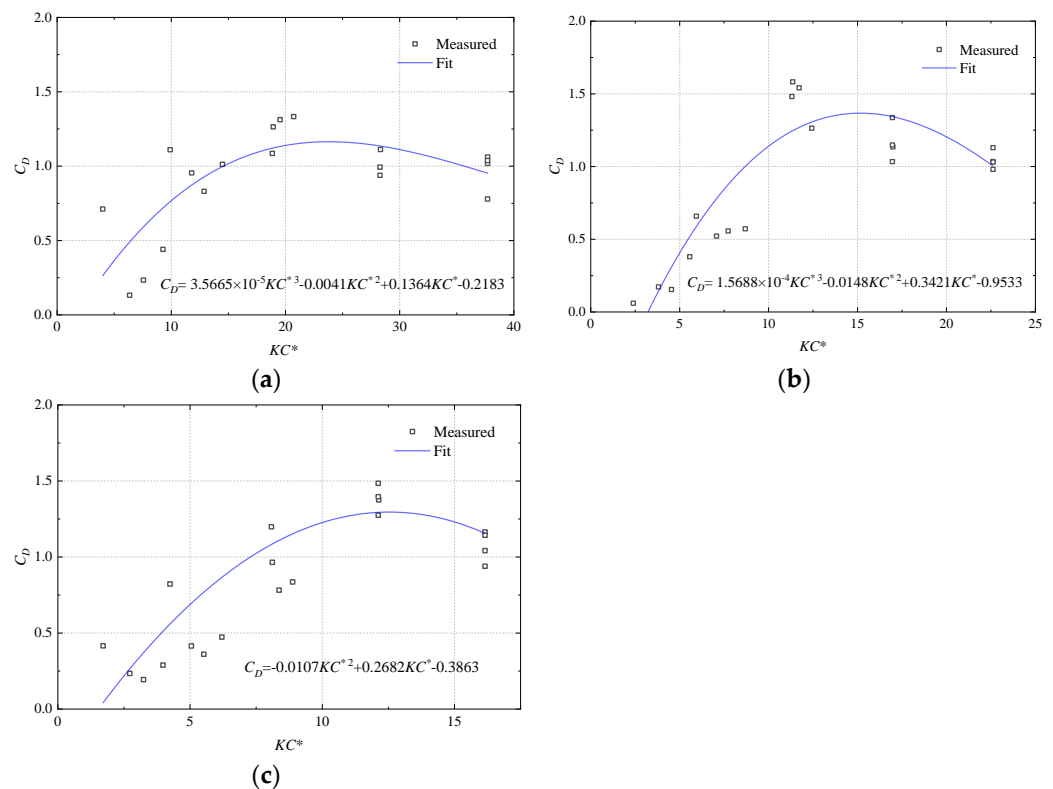
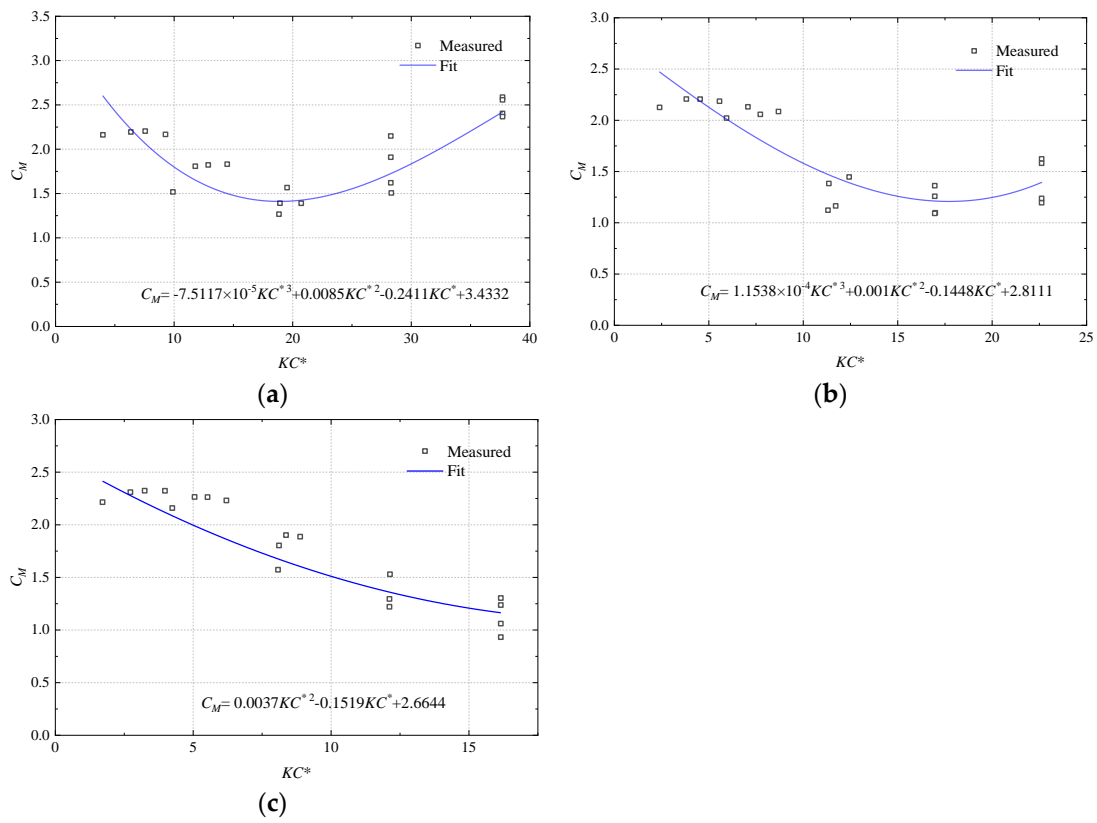
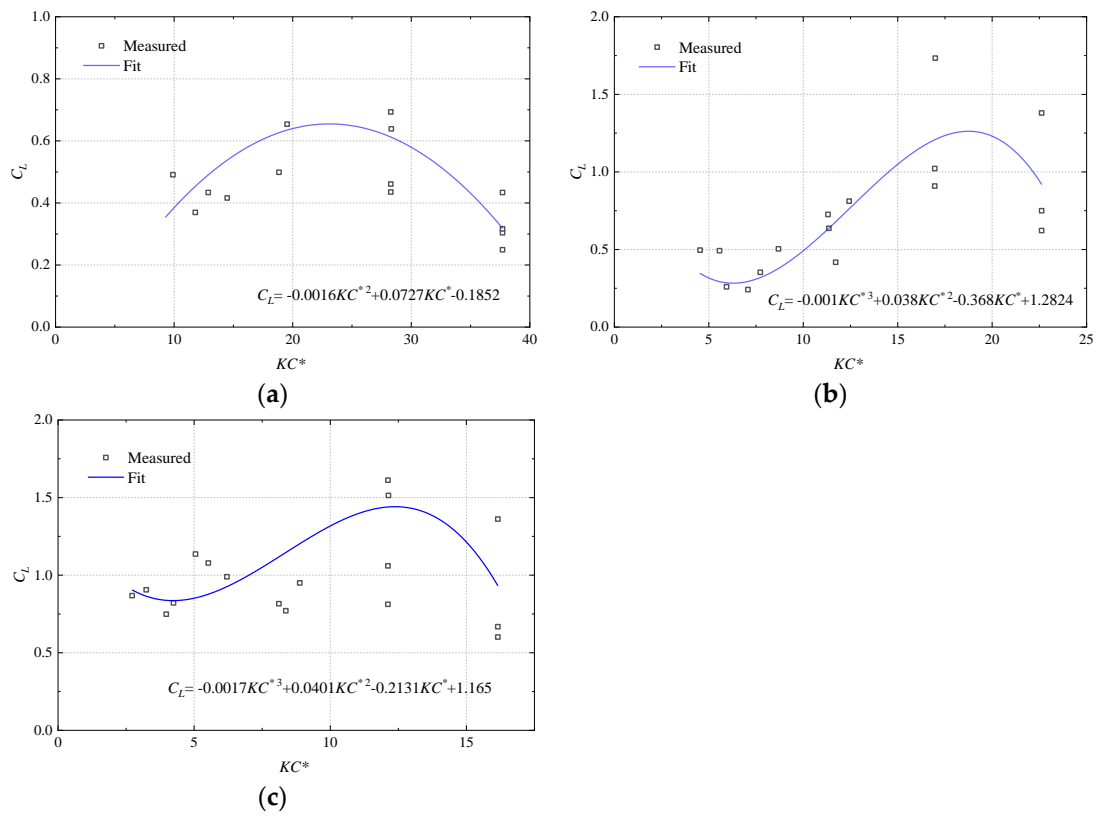


Figure 13. Drag coefficient  $C_D$  versus  $KC^*$  under wave–current action: (a)  $D = 4.5$  cm; (b)  $D = 7.5$  cm; (c)  $D = 10.5$  cm.

For the drag coefficient  $C_D$  and inertia coefficient  $C_M$ , the wave surface fluctuations in adjacent cycles are different under wave-current conditions (see Figure 5), so naturally there is also a difference in the fluctuations of the inline force in adjacent cycles (see Figure 7), and it is clear from Figure 7 that this difference becomes more obvious with increasing current velocity. Therefore, the values of  $C_D$  and  $C_M$  estimated by using the time-domain least-squares method have some discreteness.



**Figure 14.** Inertia coefficient  $C_M$  versus  $KC^*$  under wave–current action: (a)  $D = 4.5$  cm; (b)  $D = 7.5$  cm; (c)  $D = 10.5$  cm.



**Figure 15.** Lift coefficient  $C_L$  versus  $KC^*$  under wave–current action: (a)  $D = 4.5$  cm; (b)  $D = 7.5$  cm; (c)  $D = 10.5$  cm.

In addition, the distribution of  $C_D$  is similar to those of Li et al. [12] and Yuan et al. [28], who investigated the characteristics of inline forces on circular cylinders with small diameters under wave-only and wave-current conditions. For low  $KC^*$ , the inertial forces play a dominant role in the Morison formula, so the error function in the least-squares method is insensitive to any error in  $C_D$ , which is the main reason for the great fluctuation of  $C_D$  for low  $KC^*$ ; e.g., for  $KC^* < 10$ , the fluctuation of  $C_D$  for the pile with  $D = 10.5$  cm is significantly greater than that for  $KC^* > 10$ . However, these discrete  $C_D$  values for low  $KC^*$  have little impact on the total inline force predicted by the Morison formula.

It is clear from Figures 13–15 that compared with the values of  $C_D$  and  $C_M$ , those of  $C_L$  are more scattered. Using flow-visualization experiments, Iwagaki et al. [27] examined the vortices around a circular cylinder in a flow field with co-existing waves and current. For either waves only or waves and a low-speed current, pairs of symmetric vortices formed at the sides of the cylinder and caused symmetric pressure on the cylinder surface. As the current velocity increased, large asymmetric vortices continuously formed and detached at the sides of the cylinder, and these increased the complexity of the flow field and significantly increased the asymmetry of the pressure on the cylinder surface. This is reflected in the increased difference in the fluctuations of the transverse force time series between adjacent cycles (see Figure 8), resulting in a significant increase in the dispersion of  $C_L$  under the combination of waves and high current velocity, e.g., for  $KC^* > 10$ , the fluctuation of  $C_L$  for the pile with  $D = 10.5$  cm is significantly greater than that for  $KC^* < 10$ . Experimentally, Nakamura et al. [29] showed that the pressure difference caused by asymmetric vortex shedding has a significantly greater impact on the transverse force on a large-diameter cylinder than that on a small-diameter cylinder. In the present study, this is shown by the dispersion of  $C_L$  for the super-large-diameter pile ( $D = 10.5$  cm) being greater than that for the smaller-diameter pile ( $D = 4.5$  cm).

Here, the data dispersion of  $C_D$ ,  $C_M$ , and  $C_L$  as calculated from experimental data under wave-current conditions were explained in detail. This helps with analyzing the distribution of hydrodynamic coefficients more reasonably under different wave-current conditions ( $KC^*$  numbers), and it offers a necessary reference for using the modified Morison formula and Kutta–Joukowski formula to rapidly evaluate the inline and transverse forces on piles in practical engineering.

#### 4.4.2. Drag Coefficient $C_D$

Figure 13 shows that with increasing  $KC^*$  under wave-current action,  $C_D$  is well correlated with  $KC^*$ . Comparing Figure 13a–c shows that the drag coefficient  $C_D$  of the three piles increases rapidly to its peak value and then decreases slowly with increasing  $KC^*$  under wave-current action. For the piles with  $D = 10.5$  cm and 7.5 cm, the maximum value of  $C_D$  is ca. 1.5, which appears near  $KC^* \approx 12$  (Figure 13a,b). Meanwhile, for the pile with  $D = 4.5$  cm, the maximum value of  $C_D$  is ca. 1.3, which appears near  $KC^* \approx 20$  [Figure 13c], slightly less than that for the piles with  $D = 10.5$  cm and 7.5 cm. This indicates that the drag coefficient distribution ( $C_D$ – $KC^*$ ) for super-large-diameter piles is different from that for smaller-diameter piles.

#### 4.4.3. Inertia Coefficient $C_M$

Figure 14 shows that the inertia coefficient  $C_M$  is also well correlated with  $KC^*$  under wave-current action. As shown in Figure 14a,  $C_M$  for the pile with  $D = 4.5$  cm decreases and then increases for  $KC^* \approx 4$ –38, with a minimum value of ca. 1.4 near  $KC^* \approx 19$ . As shown in Figure 14b,  $C_M$  for the pile with  $D = 7.5$  cm presents a similar trend for  $KC^* \approx 2$ –22 to that of the pile with  $D = 4.5$  cm, with a minimum value of ca. 1.1 near  $KC^* \approx 17$ . Meanwhile, as shown in Figure 14c,  $C_M$  for the pile with  $D = 10.5$  cm decreases steadily from 2.4 to 1.1 for  $KC^* \approx 2$ –20 under wave-current action.

The above analysis shows that using the hydrodynamic coefficients  $C_D$  and  $C_M$  of a smaller-diameter pile and the modified Morison formula to estimate the inline wave-

current force on a super-large-diameter pile at the same  $KC^*$  would cause structural-load calculation errors and unfavorable factors.

#### 4.4.4. Lift Coefficient $C_L$

Figure 15 shows that for each of the three piles under wave–current action,  $C_L$  increases and then decreases with increasing  $KC^*$ , with the peak values for the piles with  $D = 4.5$  cm, 7.5 cm, and 10.5 cm appearing near  $KC^* = 20, 17,$  and  $12,$  respectively. The peak  $C_L$  values for the piles with  $D = 10.5$  cm and 7.5 cm are ca. 1.5 and 1.3, respectively, significantly greater than those for the pile with  $D = 4.5$  cm (ca. 0.7). This reflects the fact that piles with larger diameters have larger  $C_L$  values under the same wave–current action.

#### 4.4.5. Empirical Expressions for Hydrodynamic Coefficients

Also shown in Figures 13–15 are the curves that offer the best fit to the measured hydraulic coefficients ( $C_D, C_M,$  and  $C_L$ ) of the three piles ( $D = 4.5$  cm, 7.5 cm, and 10.5 cm). From these curves, the empirical expressions for the hydrodynamic coefficients of a super-large-diameter pile with  $D = 10.5$  cm are

$$C_D = -0.0107(KC^*)^2 + 0.2682KC^* - 0.3863 \quad (13)$$

$$C_M = 0.0037(KC^*)^2 - 0.1519KC^* + 2.6644 \quad (14)$$

$$C_L = -0.0017(KC^*)^3 + 0.0401(KC^*)^2 - 0.2131KC^* + 1.165 \quad (15)$$

To check the predictability of the above empirical expressions, the correlation coefficient  $R^2$  is calculated as

$$R^2 = 1 - \frac{\sum_{i=1}^n (C_{ie} - C_{ip})^2}{\sum_{i=1}^n (C_{ie} - \bar{C}_{ie})^2} \quad (16)$$

where  $C_{ie}$  is an experimental value of  $C_D, C_M,$  or  $C_L, \bar{C}_{ie}$  is the mean experimental value of  $C_D, C_M,$  or  $C_L, C_{ip}$  is the predicted value of  $C_D, C_M,$  or  $C_L,$  and  $n$  is the total number of observations. For Equations (13)–(15), the values of  $R^2$  are 0.8302, 0.8591, and 0.6623, respectively, indicating that these empirical expressions offer accurate and reliable predictions of the hydrodynamic coefficients ( $C_D, C_M,$  and  $C_L$ ). It also shows that Equations (13)–(15) can be used to calculate the inertial, drag, and transverse wave–current forces on the super-large-diameter pile for  $KC^* = 2$ –16.

## 5. Analysis of the Resultant Force

Although the experimental results show that there is a certain phase difference between the peak values of the transverse and inline forces under wave–current action (they generally do not occur simultaneously), the resultant force formed by the vector sum of the inline and transverse forces may still be much larger than the inline force. Under the combination of waves and a fast current in particular, the transverse force contributes significantly more to the hydrodynamic load on the pile, and the peak value of the resultant force is obviously greater than that of the inline force. This characteristic of the hydrodynamic load should be given full attention in theoretical analysis and practical engineering design.

For better quantification of how the transverse force affects the resultant force on the pile, Figures 16 and 17 show the ratio of the peak resultant force to the peak inline force ( $F_{H\_max}/F_{x\_max}$ ) and the angle  $\theta_H$  at which the peak resultant force  $F_{H\_max}$  deviates from the inline force  $F_x$  versus  $KC^*$  as induced by wave-only and wave-current actions, respectively. Figures 16 and 17 show that under the same wave-only and wave-current actions,  $F_{H\_max}/F_{x\_max}$  and  $\theta_H$  for different pile diameters have their own significant ranges of  $KC^*$ . In this study, the range of  $KC^*$  corresponding to  $F_{H\_max}/F_{x\_max} > 1.1$  is defined as the significant interval for the resultant force, while that corresponding to  $F_{H\_max}/F_{x\_max} \leq 1.1$  is defined as the insignificant interval for the resultant force.

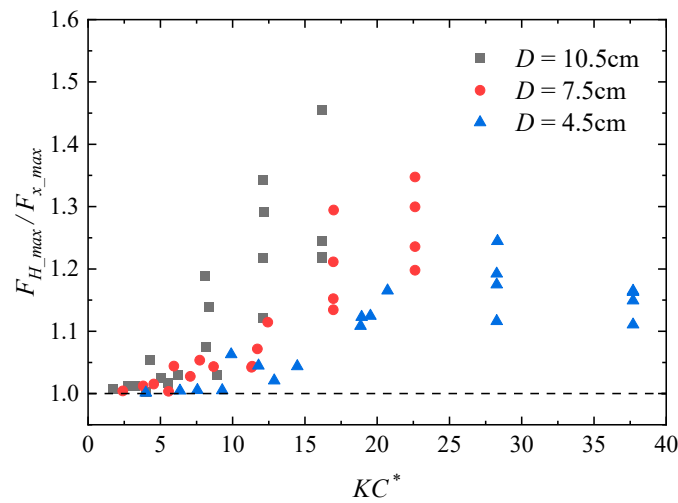


**Figure 16.** Ratio of peak resultant force to peak inline force.

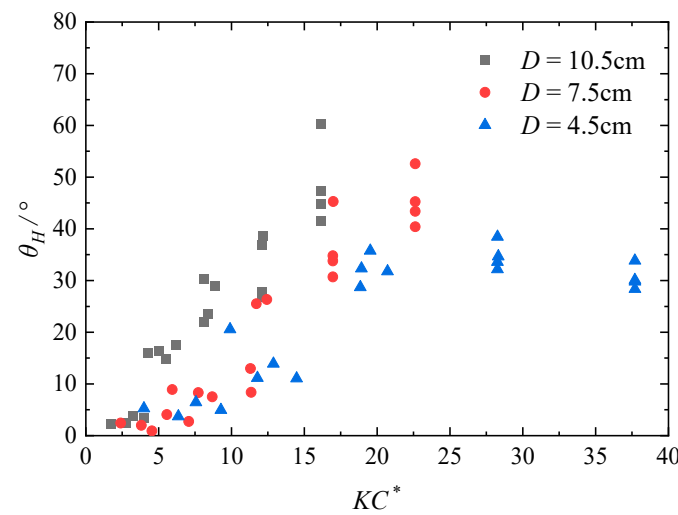


**Figure 17.** Angle between the direction of the peak resultant force and the incident direction of waves and current.

For the super-large-diameter pile with  $D = 10.5$  cm,  $F_{H\_max}/F_{x\_max}$  and  $\theta_H$  increase with increasing  $KC^*$ . The  $F_{H\_max}/F_{x\_max}$  values for  $KC^* \approx 8$ – $16$  are larger than those for  $KC^* < 8$ , exceeding 1.1 in most cases, and similarly  $\theta_H$  is larger, with all values exceeding  $20^\circ$ . At  $KC^* \approx 16$ ,  $F_{H\_max}/F_{x\_max}$  reaches its maximum value of 1.45, while  $\theta_H$  also achieves its maximum value of  $60^\circ$ .

For the pile with  $D = 7.5$  cm, the distribution trend is similar to that for the pile with  $D = 10.5$  cm, and both  $F_{H\_max}/F_{x\_max}$  and  $\theta_H$  increase with increasing  $KC^*$ . The larger values of  $F_{H\_max}/F_{x\_max}$  and  $\theta_H$  are distributed mainly in  $KC^* \approx 12$ – $23$ . At  $KC^* \approx 23$ ,  $F_{H\_max}/F_{x\_max}$  and  $\theta_H$  reach their maximum values of about 1.35 and  $52^\circ$ , respectively.

For the pile with  $D = 4.5$  cm and increasing  $KC^*$ ,  $F_{H\_max}/F_{x\_max}$  and  $\theta_H$  increase for  $KC^* \leq 28$  but decrease for  $KC^* > 28$ , reaching their maximum values of ca. 1.24 and  $38^\circ$ , respectively, at  $KC^* \approx 28$ . Overall, the significant range of  $KC^*$  for  $F_{H\_max}/F_{x\_max}$  and  $\theta_H$  is  $KC^* \approx 19$ – $38$ .

The analysis of the ratio of the peak resultant and inline forces ( $F_{H\_max}/F_{x\_max}$ ) and the angle  $\theta_H$  between the resultant force and the incident flow direction in Table 2 shows further that the  $F_{H\_max}/F_{x\_max}$  and  $\theta_H$  values for the three piles are close in their insignificant  $KC^*$  intervals. However, in their significant  $KC^*$  intervals, the values of  $F_{H\_max}/F_{x\_max}$  and  $\theta_H$  for the super-large-diameter pile with  $D = 10.5$  cm are significantly greater than those of the small-diameter pile with  $D = 4.5$  cm.

**Table 2.** Comparison of resultant and inline forces on different piles.

Pile	Mean $F_{H\_max}/F_{x\_max}$	Mean $\theta_H$ [°]	Significant Interval			Insignificant Interval		
			KC*	Mean $F_{H\_max}/F_{x\_max}$	Mean $\theta_H$ [°]	KC*	Mean $F_{H\_max}/F_{x\_max}$	Mean $\theta_H$ [°]
D = 10.5 cm	1.14	25	8–16	1.23	36	0–8	1.02	11
D = 7.5 cm	1.12	24	12–23	1.22	37	0–12	1.03	8
D = 4.5 cm	1.10	24	19–38	1.15	32	0–19	1.02	9

Notes: mean  $F_{H\_max}/F_{x\_max}$ —mean value of ratio of peak resultant force to peak inline force ( $F_{H\_max}/F_{x\_max}$ ); mean  $\theta_H$ —mean value of angle (°) at which peak resultant force  $F_{H\_max}$  deviates from inline force  $F_x$ .

Comparing Figures 15–17 shows that the significant range of  $KC^*$  for  $F_{H\_max}/F_{x\_max}$  and  $\theta_H$  for each pile corresponds to that in which  $C_L$  is larger. Therefore, within a certain range of  $KC^*$ , the influence of the transverse force on the peak value and direction of the resultant force cannot be ignored. This is particularly obvious under strong waves and currents. Furthermore, note that under the same wave-current action, the transverse force contributes more to the hydrodynamic load on a super-large-diameter pile than that on a small-diameter pile, making it easier to excite extreme structural loads. Therefore, in engineering design, the simplified method of taking the maximum inline force as the design hydrodynamic load is applicable only to a pile with a relatively small diameter and in its corresponding insignificant  $KC^*$  interval. In that case,  $F_{H\_max}/F_{x\_max}$  generally does not exceed 1.1 and  $\theta_H$  is less than 20°, so no excessive errors are generated. However, for a super-large-diameter pile, it is necessary to consider the influence of the transverse force when designing its hydrodynamic loads under combined wave-current action.

### 6. Conclusions

Herein, the prototype was one of the 6.3-m super-large-diameter piles of the Xihoumen Rail-cum-Road Bridge, and an experimental study was reported of the hydrodynamic loads on a super-large-diameter pile under wave-only and wave-current actions. Wide ranges of wave height and current velocity were used to measure the inline and transverse forces on three piles ( $D = 4.5$  cm, 7.5 cm, and 10.5 cm). The drag, inertia, and lift coefficients of the piles were calculated based on the modified Morison formula, Kutta–Joukowski formula, and linear wave theory, and the influence of the transverse force on the resultant force on the piles was also analyzed. The main conclusions are summarized below.

In deep-water conditions, for waves and current propagating in the same direction, the wave height decreases as the current velocity increases. In the experiments, the influence of high velocity on the wave height was very obvious, and at  $U = 0.4$  m/s, the wave height decreases by more than  $0.3 H_0$ . While the wave period remains mostly unaffected by the increase in current velocity.

Both current velocity and wave height have a significant impact on the hydrodynamic loads on a super-large-diameter pile, with the inline and transverse forces obviously increasing with increasing current velocity and wave height. In addition, compared with the wave-only-induced inline and transverse forces, the fluctuation amplitude of the wave-current-induced inline force decreases greatly with increasing current velocity, whereas that of the wave-current-induced transverse force increases rapidly. Under strong waves and currents, the peak value of the transverse force can reach tens of times that induced by wave-only action, becoming of the same level as the inline force.

The drag coefficient  $C_D$ , inertia coefficient  $C_M$ , and lift coefficient  $C_L$  are well correlated with  $KC^*$  under wave-only and wave-current actions. Corresponding empirical expressions for the hydrodynamic coefficients  $C_D$ ,  $C_M$ , and  $C_L$  of the super-large-diameter pile for  $KC^* \approx 2$ –16 was proposed from fitting the experimental data, and these expressions can be used to quickly estimate the inline and transverse forces acting on a super-large-diameter pile in deep water.

Compared with the small-diameter pile with  $D = 4.5$  cm, the inline and transverse wave-current forces on the super-large-diameter pile with  $D = 10.5$  cm increase more

significantly with increasing current velocity and wave height. Similarly, under the same wave-current conditions, the peak values of  $C_D$  and  $C_M$  for the super-large-diameter pile are slightly larger than those for the small-diameter pile, while the peak value of  $C_L$  can become more than twice that for the small-diameter pile.

The present study indicates that although the peak values of the inline and transverse forces on a super-large-diameter pile have a certain phase difference under wave-current conditions, the influence of the transverse force on the resultant force cannot be ignored in the significant range of  $KC^*$  (the range in which  $C_L$  is larger). The ratio of the peak resultant and inline forces  $F_{H\_max}/F_{x\_max}$  and the angle  $\theta_H$  of the peak resultant force  $F_{H\_max}$  deviating from the inline force can reach 1.45 and  $60^\circ$ , respectively. The contribution of the transverse force to the hydrodynamic load on the super-large-diameter pile is more significant than that on the small-diameter pile, making it easier to trigger extreme structural loads. Therefore, it is necessary to consider the influence of the transverse force when designing the hydrodynamic loads on large-diameter piles under combined wave-current action.

**Author Contributions:** Conceptualization, Z.L.; Data curation, C.H.; Formal analysis, L.W.; Funding acquisition, Z.L. and F.W.; Methodology, C.H.; Project administration, Z.Z.; Resources, Z.L. and Z.Z.; Validation, F.W. and L.W.; Writing—original draft, C.H.; Writing—review and editing, Z.L. All authors have read and agreed to the published version of the manuscript.

**Funding:** This research was funded by the Major Special Science and Technology Project of “Ningbo Science and Technology Innovation 2025”, grant number 2019B10076, and The Natural Science Foundation of Zhejiang Province, grant number LY23E080001).

**Institutional Review Board Statement:** Not applicable.

**Informed Consent Statement:** Not applicable.

**Data Availability Statement:** The data supporting this study have been provided within this paper.

**Acknowledgments:** This model test was conducted in the Laboratory of Offshore Engineering at Zhejiang University.

**Conflicts of Interest:** The authors declare no conflict of interest.

## References

1. Li, C.-W.; Lin, P. A numerical study of three-dimensional wave interaction with a square cylinder. *Ocean Eng.* **2001**, *28*, 1545–1555. [[CrossRef](#)]
2. Mo, W.; Irschik, K.; Oumeraci, H.; Liu, P.L.F. A 3D numerical model for computing non-breaking wave forces on slender piles. *J. Eng. Math.* **2006**, *58*, 19–30. [[CrossRef](#)]
3. Huang, Z.; Xu, C.; Huang, S. A CFD simulation of wave loads on a pile-type oscillating-water-column device. *J. Hydrodyn.* **2019**, *31*, 41–49. [[CrossRef](#)]
4. Male, P.V.; Vergassola, M.; Dalen, K.V. Decoupled modelling approaches for environmental interactions with monopile-based offshore wind support structures. *Energies* **2020**, *13*, 5195. [[CrossRef](#)]
5. Tsetas, A.; Tsouvalas, A.; Metrikine, A.V. Installation of large-diameter monopiles: Introducing wave dispersion and non-local soil reaction. *J. Mar. Sci. Eng.* **2021**, *9*, 313. [[CrossRef](#)]
6. Morison, J.R.; O'Brien, M.P.; Johnson, J.W.; Schaaf, S.A. The force exerted by surface waves on piles. *J. Pet. Technol.* **1950**, *2*, 149–154. [[CrossRef](#)]
7. Sarpkaya, T.; Storm, M. In-line force on a cylinder translating in oscillatory flow. *Appl. Ocean. Res.* **1985**, *7*, 188–196. [[CrossRef](#)]
8. Yu, Y.; Miao, X. The transverse force of waves acting on vertical pile. *Acta Oceanol. Sin.* **1989**, *11*, 248–261.
9. Ren, Z. Calculation of wave-current force on isolated pile. *Acta Oceanol. Sin.* **1984**, *3*, 574–586.
10. Wolfram, J.; Naghipour, M. On the estimation of Morison force coefficients and their predictive accuracy for very rough circular cylinders. *Appl. Ocean. Res.* **1999**, *21*, 311–328. [[CrossRef](#)]
11. Li, Y. Aspect of the normalization of hydrodynamic coefficients in Morison equation. *J. Hydrodyn.* **1998**, *13*, 329–337.
12. Li, Y.; Wang, F.; Kang, H. Wave-current forces on slender circular cylinders. *China Ocean. Eng.* **1991**, *5*, 287–310.
13. Wan, D.; Liu, Y.; Miao, G. The interactions between wave-currents and offshore structures with consideration of fluid viscosity. *ACTA Mech. Sin.* **1996**, *12*, 307–322.
14. Tung, C.C.; Huang, N.E. Combined effects of current and waves on fluid force. *Ocean. Eng.* **1973**, *2*, 183–193. [[CrossRef](#)]

15. Ghadirian, A.; Vested, M.H.; Carstensen, S.; Christensen, E.D.; Bredmose, H. Wave-current interaction effects on waves and their loads on a vertical cylinder. *Coast. Eng.* **2021**, *165*, 103832. [[CrossRef](#)]
16. Kang, A.; Zhu, B. Wave-current interaction with a vertical square cylinder at different reynolds numbers. *J. Mod. Transp.* **2013**, *21*, 47–57. [[CrossRef](#)]
17. Sundar, V.; Vengatesan, V.; Anandkumar, G.; Schlenkhoff, A. Hydrodynamic coefficients for inclined cylinders. *Ocean. Eng.* **1998**, *25*, 277–294. [[CrossRef](#)]
18. Qu, S.; Liu, S.; Chen, O.; Sun, S.; Ren, H. Numerical simulation of breaking wave loading on standing circular cylinders with different transverse inclined angles. *Appl. Sci.* **2020**, *10*, 1347. [[CrossRef](#)]
19. Corvaro, S.; Crivellini, A.; Marini, F.; Cimorelli, A.; Capitanelli, L.; Mancinelli, A. Experimental and numerical analysis of the hydrodynamics around a vertical cylinder in waves. *J. Mar. Sci. Eng.* **2019**, *7*, 453. [[CrossRef](#)]
20. Corvaro, S.; Marini, F.; Mancinelli, A.; Lorenzoni, C.; Brocchini, M. Hydro- and morpho-dynamics induced by a vertical slender pile under regular and random waves. *J. Waterw. Port Coast. Ocean. Eng.* **2018**, *144*, 04018018.1–04018018.19. [[CrossRef](#)]
21. Miles, J.; Martin, T.; Goddard, L. Current and wave effects around windfarm monopile foundations. *Coast. Eng.* **2017**, *121*, 167–178. [[CrossRef](#)]
22. Chen, L.-F.; Ning, D.-Z.; Teng, B.; Zhao, M. Numerical and experimental investigation of nonlinear wave-current propagation over a submerged breakwater. *J. Eng. Mech.* **2017**, *143*, 04017061. [[CrossRef](#)]
23. Kang, A.; Zhu, B.; Lin, P.; Ju, J.; Zhang, D. Experimental and numerical study of wave-current interactions with a dumbbell-shaped bridge cofferdam. *Ocean. Eng.* **2020**, *210*, 107433. [[CrossRef](#)]
24. Li, Y.C.; Herbich, J.B. Effect of wave-current interaction of the wave parameter. In Proceedings of the 18th International Conference on Coastal Engineering, Cape Town, South Africa, 29 January 1980; pp. 413–438.
25. Iwagaki, Y.; Sakai, T.; Tsuda, T.; Oka, Y. Wave refraction and wave height variation due to current. *Bull. Disaster Prev. Res. Inst.* **1977**, *27*, 73–91.
26. Hedges, T.S.; Lee, B.W. The equivalent uniform current in wave-current computation. *Coast. Eng.* **1992**, *16*, 301–311. [[CrossRef](#)]
27. Iwagaki, Y.; Asano, T. Hydrodynamic forces on a circular cylinder due to combined wave and current loading. In Proceedings of the 19th International Conference on Coastal Engineering, Houston, TX, USA, 3–7 September 1984; pp. 2857–2914.
28. Yuan, Z.; Huang, Z. An experimental study of inertia and drag coefficients for a truncated circular cylinder in regular waves. *J. Hydrodyn.* **2010**, *22*, 318–323. [[CrossRef](#)]
29. Nakamura, M.; Hoshino, K.; Koterayama, W. Three dimensional effects on hydrodynamic forces acting on an oscillating finite-length circular cylinder. *Int. J. Offshore Polar Eng.* **1992**, *2*, 81–86.

**Disclaimer/Publisher’s Note:** The statements, opinions and data contained in all publications are solely those of the individual author(s) and contributor(s) and not of MDPI and/or the editor(s). MDPI and/or the editor(s) disclaim responsibility for any injury to people or property resulting from any ideas, methods, instructions or products referred to in the content.